



ChemComm

**Formation of Choline Salts and Dipolar Ions for CO₂
Reactive Eutectic Solvents**

Journal:	<i>ChemComm</i>
Manuscript ID	CC-COM-07-2023-003272.R2
Article Type:	Communication

SCHOLARONE™
Manuscripts

COMMUNICATION

Formation of Choline Salts and Dipolar Ions for CO₂ Reactive Eutectic Solvents

Received 00th January 20xx,
Accepted 00th January 20xx

Ruth Dikki^a, Eda Cagli^a, Drace Penley^a, Metin Karayilan^b, Burcu Gurkan^{*a}

DOI: 10.1039/x0xx00000x

Choline-based sorbents derived from imidazole (ImH), phenol (PhOH), pyrrole-2-carbonitrile (CNpyrH), and 1,2,4-triazole (TrzH) are developed for CO₂ capture to enable alternative regeneration approaches over aqueous amines. During synthesis, the equilibrium between [Ch]⁺[OH]⁻ and Ch[±] dipolar in water shifts to support the formation of Ch[±]ImH and Ch[±]PhOH in the presence of ImH and PhOH upon drying. Whereas, salts of [Ch]⁺[CNpyr]⁻ and [Ch]⁺[Trz]⁻ were obtained with CNpyrH and TrzH, as confirmed by NMR and FTIR spectroscopy. Density functional theory (DFT) calculations support a spontaneous proton transfer from CNpyrH and TrzH to Ch[±] while it shows an energy barrier in the case of ImH. These sorbents formed eutectic solvents upon mixing with ethylene glycol (EG) where deprotonation of EG and subsequent binding of CO₂ contributed to capacities up to 3.56 mol CO₂/kg at 25 °C and 1 bar of CO₂. The regenerability of the eutectic solvents was demonstrated by dielectric heating via microwave (MW) in support of renewable energy utilization. This study shows the impact of proton sharing on the CO₂ capacity and regenerability of eutectic sorbents as molecular design guidance.

The growing demand for green solvents has led to a rising interest in eutectic solvents, which are composed of a hydrogen bond acceptor (HBA) and a hydrogen bond donor (HBD) forming strong hydrogen bonding networks.¹ The tunable and benign nature of eutectic solvents makes them appealing for various applications particularly for separations.²⁻⁵ A major driver for the recent surge in eutectic solvent research for low-pressure CO₂ separations is their appreciable CO₂ capacities, attainable when functionalized with nucleophilic sites for CO₂ chemisorption.^{5,6} Choline-based eutectic solvents, particularly those containing biodegradable choline chloride ([Ch]⁺[Cl]⁻), are readily available and can be derivatized for specific applications.⁷ Ethaline is a common example of a eutectic solvent composed of [Ch]⁺[Cl]⁻ and EG (about 1:4 molar ratio).⁸ While ethaline has no CO₂ chemisorption capacity, anion functionalization, such as replacing the [Cl]⁻ anion with proline [Pro]⁻ or glycinate [Gly]⁻, results in the formation of CO₂ reactive eutectic solvents,^{5,9} with CO₂ binding to the anion, but not to [Ch]⁺ or EG. These functionalized solvents present

appreciable CO₂ capacities at low partial pressures,^{6,9-11} which is ideal for CO₂ capture applications, such as direct air capture.

The addition of EG to viscous ionic liquids (ILs)^{2,5} or solid organic salts^{6,7} for the formation of eutectic solvents enhances CO₂ transport properties. However, in the presence of anions that are strong HBAs, EG was reported to deprotonate and provide an alternative binding site for CO₂.^{2,11} There are only a few examples of CO₂-reactive eutectic solvents and the understanding of how the CO₂ capacities as well as solvent regenerability depend on the hydrogen bonding network is not well-developed. In this study, the anion exchange and proton transfer reactions leading to sorbent development and CO₂ binding to the derivatized choline-based eutectic solvents were examined. Table S1 shows the eutectic solvent components, their molecular structures, and known pK_a values in aqueous and nonaqueous systems. The anion precursors examined have an amine or alcohol moiety that theoretically present available binding sites for CO₂ upon deprotonation. The developed eutectic solvents were characterized by NMR and FTIR spectroscopy, and thermal analysis was conducted by employing differential scanning calorimetry (DSC) and thermogravimetric analysis (TGA). CO₂ absorption capacities and solvent regenerability were studied to assess their applicability for CO₂ capture applications. To understand the chemisorption of CO₂, NMR techniques were performed and the energetics of the proposed reactions including the proton transfers were confirmed by DFT calculations. The results present a different mechanistic insight than the previous reports for similar eutectic solvents. Further, we present the feasibility of regeneration via dielectric heating by the application of MW as an alternative to convective thermal heating.

Following the commonly applied IL synthesis procedure,¹² solid amine and alcohol functionalized HBAs were obtained. **Figure 1a** shows the reaction steps involved in the formation of [Ch]⁺[Trz]⁻ and Ch[±]ImH as specific examples. The chloride to hydroxide anion exchange process in step 1 generates choline hydroxide ([Ch]⁺[OH]⁻) in equilibrium with choline dipolar ion (Ch[±]) and water. With the addition of TrzH (pK_a = 9.97 in H₂O)¹³ to the solution, [Ch]⁺[Trz]⁻ salt was obtained upon drying. Similarly, in the case of CNpyrH, the acid-base neutralization reaction in step 2 yielded [Ch]⁺[CNpyr]⁻ salt. However, with the more basic ImH (pK_a = 14.52 in H₂O),¹³ a change in the proton acidity in step 2 favors the protonation of [Im]⁻ over

^a Department of Chemical and Biomolecular Engineering, Case Western Reserve University, Cleveland, OH.

^b Department of Chemistry, Case Western Reserve University, Cleveland, OH
Electronic Supplementary Information (ESI) available: [details of any supplementary information available should be included here]. See DOI: 10.1039/x0xx00000x

Ch^\pm , thus preferentially forming solid Ch^\pmImH sorbent upon drying. The formation of Ch^\pmImH is possible because $[\text{Ch}]^+$ is a weak Bronsted-Lowry acid that sparingly loses its hydroxyl proton to form Ch^\pm with a reported $\text{p}K_b$ value of 0.1 in water,¹⁴ compared to -0.52 for $[\text{Im}]^-$. A similar case was observed with PhOH where Ch^\pmPhOH was obtained as a solid sorbent.

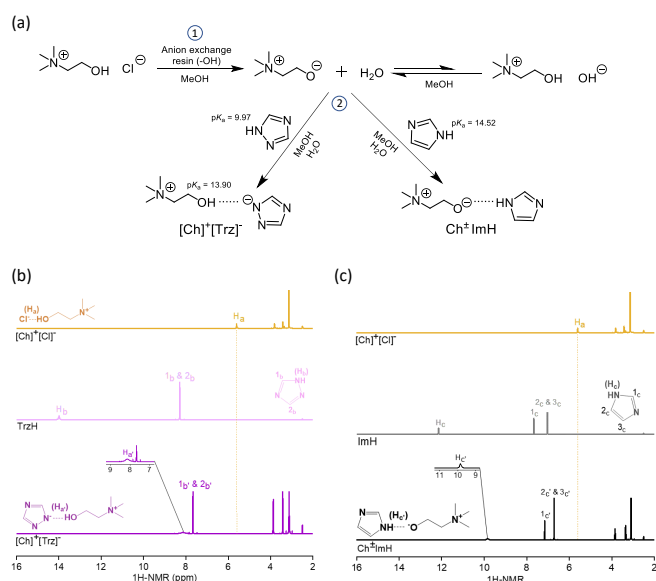


Figure 1. (a) The synthesis of $[\text{Ch}]^+[\text{Trz}]^-$ salt and Ch^\pmImH sorbent. The dotted lines represent intermolecular proton sharing and hydrogen bonding interactions. (b) and (c) represent ¹H-NMR spectra of (b) $[\text{Ch}]^+[\text{Trz}]^-$ and (c) Ch^\pmImH and their corresponding precursors in DMSO-d₆. The peaks with low signal intensities are shown in the insets (H_a and H_c both integrate to approximately 1).

The example ¹H-NMR spectra highlighting the chemical shifts of the -OH/-NH protons of $[\text{Ch}]^+[\text{Trz}]^-$ and Ch^\pmImH in comparison to the starting materials of $[\text{Ch}]^+[\text{Cl}]^-$ (H_a), TrzH (H_b), and ImH (H_c) is given in **Figures 1b** and **c** (see also **Figures S1-S3**). During synthesis, TrzH was deprotonated, and therefore, the signal for H_b is absent (**Figure 1b**). Similar is true for $[\text{Ch}]^+[\text{CNpyr}]^-$, consistent with previous reports involving synthesis of imidazolium-based ILs.¹⁵ Consequently, -OH proton of $[\text{Ch}]^+$ experiences a downfield shift of about 2.53 ppm when $[\text{Cl}]^-$ counter ion is replaced with $[\text{Trz}]^-$. In contrast to TrzH and CNpyrH , weaker proton donors PhOH and ImH did not appear to be deprotonated after a similar synthesis procedure. The NMR signal of H_c (9.8 ppm) is attributed to the -NH proton on ImH H-bonding with Ch^\pm as shown in the inset (-NH...O) (**Figure 1c**). The build-up of electron density on ImH in Ch^\pmImH within the DMSO-d₆ solution results from proton sharing between ImH and Ch^\pm conjugate base with high proton affinity that allows for the formation Ch^\pmImH in equilibrium with the less favorable $[\text{Ch}]^+[\text{Im}]^-$. Increased electron density resulting from charge spreading to an uncharged molecule/functional group has been shown to accompany strong proton sharing and hydrogen bonding interactions.^{16,17}

Contrary to our observations, *Li et al.*¹⁸ and *Nie et al.*¹⁹ reported the formation of $[\text{Ch}]^+[\text{Im}]^-$ and $[\text{Ch}]^+[\text{PhO}]^-$, respectively, which we suspect to result from the high-water content. When the ¹H-NMR chemical shifts of the Ch^\pmImH sample were probed after adding 10 wt% water, H_b peak associated with -NH...O, experienced an upfield shift from 9.85 ppm to 6.03 ppm as seen in **Figure S4**. This chemical shift is more consistent with the ¹H-

NMR analysis by *Li et al.* A chemical shift was observed from 1.10 ppm to 3.80 ppm accompanied by an increase in the peak integration, therefore indicating the presence of more hydrogen-bonding protons from water. Since NMR analysis alone is not sufficient to differentiate $[\text{Im}]^-$ from ImH and $[\text{PhO}]^-$ from PhOH in the presence of proton sharing, further examination with FTIR spectroscopy and DFT calculations were performed.

The local FTIR spectra shown in **Figure S5** (full spectra in **Figure S6**) confirm the lack of O-H stretching vibration for Ch^\pmImH and instead present sharp peaks at 3106 cm⁻¹ and 3124 cm⁻¹ that are consistent with the N-H/C-H (unsaturated) stretching vibrations. For comparison, the presence of the -OH in $[\text{Ch}]^+[\text{Trz}]^-$ is evident by the broad peak around 3115 cm⁻¹ in **Figure S5**, which is consistent with the O-H stretching vibration. Similar observations of dipolar ion formation and hydrogen bonding with the aromatic protons on PhOH were made. Although PhOH is more acidic than $[\text{Ch}]^+$ in water, we believe PhOH to be slightly more favorably protonated in Ch^\pmPhOH because of its decreased acidity in a nonaqueous system (PhOH $\text{p}K_a$ in DMSO = 18.0),²⁰ similar to ImH ($\text{p}K_a$ in DMSO = 18.6).²¹

To support the interpretation of the dipolar ion coexistence with ImH and PhOH , DFT calculations evaluating the energetics of proton transfer between the HBA and HBD components were performed (**Table S2**). Specifically, the energy that is required to move a proton from ImH to Ch^\pm is found to be positive (+3.7 kcal/mol), suggesting the formation of $[\text{Ch}]^+[\text{Im}]^-$ to be unfavourable over Ch^\pmImH . However, for TrzH and CNpyrH , the Gibbs free energy difference is significantly more negative (-16.9 and -16.3 kcal/mol), suggesting that the proton transfer is spontaneous, hence the formation of the salts is not surprising. For PhOH , the energy required for a similar proton transfer is smaller (-2.5 kcal/mol; comparable to the uncertainty of calculations when considering multiple basis sets). To further probe the interactions in the presence of solvating molecules, both $[\text{Ch}]^+[\text{PhO}]^-$ and Ch^\pmPhOH were examined with additional EG molecules. The geometry optimization calculations revealed the preferential binding of the proton to $[\text{PhO}]^-$ and convergence to Ch^\pmPhOH with hydrogen bonding to EG molecules as shown in **Figure S7**.

Experimentally, when the synthesized solid sorbents were further mixed with EG, in 1:2 molar ratio, eutectic solvents with CO₂ chemisorbing capability were developed. The DSC curves (**Figure S8**) did not present any melting or crystallization features for these mixtures in the temperature range examined (40 to -120 °C) at a 10 °C/min ramping rate; however, an endothermic peak that was assigned to the glass transition was consistently seen for all of the mixtures with EG. Due to the existence of a dynamic H-bonding network, it is not surprising that melting and crystallization are not captured at such high-temperature ramp rate. However, the existence of a glass transition is indicative of a low-transition temperature mixture and suggests the presence of metastable polymorphs that is characteristic of eutectic solvents. The TGA curve (**Figure S9**) indicates the eutectic solvents to be thermally stable up to 100-120 °C, beyond which evaporation due to EG becomes significant (> 5wt%; see **Table S3** for onset temperatures). The chemisorption of CO₂ by the prepared solvents was confirmed by ¹³C-NMR spectroscopy (**Figure 2a**). The product distribution analysis (**Figure 2b**) and the quantified CO₂ capacities (**Figure 2c**)

indicate the occurrence of proton transfer between the HBAs and EG HBD. Both the CO₂ capacities and the product distribution were observed to be dependent on: (i) the pK_b of the conjugate base in HBA, (ii) the localization of electron density of the functional components of the eutectic solvents, and (iii) the mole ratio of EG. Bicarbonate product (A) forms as a result of CO₂ reaction with the trace amount of water present or absorbed by the eutectic solvents, whereas the carbamate (C) and carbonate products (B, D, and E) form as a result of CO₂ binding to [Im]⁻ (C), Ch[±] (B), and EG (D and E), with EG carbonate being the major route in all the samples.

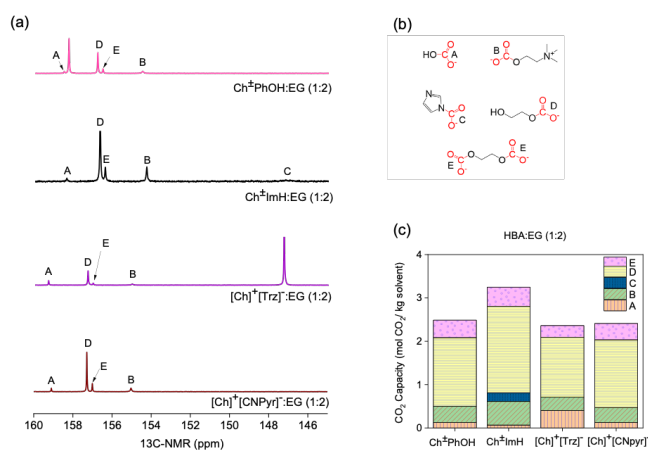


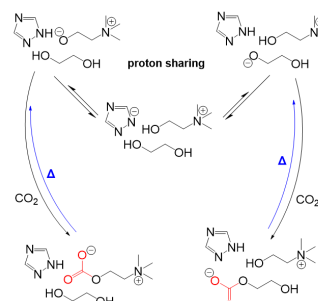
Figure 2. CO₂ saturated EG-based eutectic solvents with Ch[±]PhOH, Ch[±]ImH, [Ch]⁺[Trz]⁻, and [Ch]⁺[CNpyr]⁻ HBAs showing (a) ¹³C-NMR spectra of the chemisorbed CO₂, (b) CO₂ binding sites determined from 1D- and 2D-NMR analyses (see Figure S10), and (c) quantified CO₂ gravimetric capacities and product distributions obtained at 1 bar of CO₂ and at 25 °C in DMSO-d₆. Water content measured by Karl-Fischer titrator was 3100, 1500, 5200, and 3800 ppm for Ch[±]PhOH, Ch[±]ImH, [Ch]⁺[Trz]⁻, and [Ch]⁺[CNpyr]⁻ eutectics, respectively.

The higher mole percent of CO₂ bound to the oxygen atom in EG compared to that in Ch[±] could result from the decreased electron density (and increased stability of O⁻) that accompanies the delocalization of its electron density (see NMR spectra in Figure S11 for comparison), by inductive effect brought on by the ammonium group.²² The higher EG-CO₂ interaction could also be attributed to the presence of more CO₂ binding sites on EG than Ch[±]. The impact of different EG mole ratios on the product distribution is shown for the Ch[±]ImH:EG (1:1, 1:2, and 1:3) samples in Figure S12. The relative mole percent of CO₂ covalently bound to EG was observed to increase from 53% to 75% to 85% when the Ch[±]Im:EG molar ratio was varied from 1:1 to 1:2 to 1:3, respectively, while the mole percent of CO₂ bound to Ch[±] decreased from 24% to 17% to 9%, respectively. Similarly, resonance in [Im]⁻, [PhO]⁻, [Trz]⁻, and [CNpyr]⁻ delocalizes their electron density compared to EG and Ch[±].²³ Therefore, adducts of [PhO]⁻-CO₂, [Trz]⁻-CO₂, and [CNpyr]⁻-CO₂ were undetectable, while adducts of [Im]⁻-CO₂ (product C) yielded only 14, 6, and 0% in Ch[±]ImH:EG eutectics with 1:1, 1:2, and 1:3 molar ratios, respectively. The decrease in the Ch[±]-CO₂ and [Im]⁻-CO₂ interactions result from the increase in the number of protons and hydrogen bonds that occupy the CO₂ reactive sites, therefore making them less nucleophilic, and less CO₂ reactive. Whereas the initial increase in the total moles of CO₂ bound to EG from 0.44 to 0.72 moles in the 1:1 and 1:2 eutectics results from an increase in the CO₂ binding sites on EG. Further increase in EG content in 1:3 mixtures did not increase capacity further since it enhanced EG-EG interactions, thus

hindering access to reactive sites. It was found that the CO₂ capacity due to binding to choline (B) and EG (D+E) depended linearly on the pK_b of the HBA in 1:2 mixtures (Figure S13). This is evident from the increase in capacity when [Im]⁻ (ImH pK_a = 18.6 in DMSO) was replaced with [Trz]⁻ (TrzH pK_a = 13.9 in DMSO). Similarly, replacing [Trz]⁻ with [Cl]⁻ (HCl pK_a = 1.8 in DMSO), resulted in no detected chemisorption of CO₂ to EG due to increasing in the charge stability with [Cl]⁻. This increasing charge stability is accompanied by a decrease in its proton affinity and a decrease in the number of nucleophilic sites created on choline and EG for CO₂ chemisorption through proton sharing.

Scheme 1 illustrates the CO₂ absorption and desorption in [Ch]⁺[Trz]⁻:EG eutectic solvent as interpreted from NMR analysis. Figure S14 shows the corresponding quantitative ¹³C-NMR spectrum of TrzH and [Ch]⁺[Trz]⁻:EG (1:2), with and without CO₂. Overlapping carbon peaks (1_b' and 2_b' at 148.8 ppm) in the neat eutectic solvent experiences an upfield shift (147.3 ppm) after CO₂ chemisorption, which is closer in proximity to carbons 1_b and 2_b in TrzH (147.0 ppm). In the CO₂ saturated [Ch]⁺[Trz]⁻:EG (1:2), [Trz]⁻ exists primarily in its protonated form as TrzH. This was similarly observed with the Ch[±]ImH:EG (1:2) eutectic solvent where [Im]⁻ was observed to exist primarily in its protonated form upon CO₂ saturation (Figure S15; Scheme S1 illustrates the CO₂ binding reactions). This is expected because the resulting conjugate bases post CO₂ chemisorption have low proton affinity for strong proton sharing. With 10wt% water, bicarbonate increases as seen in NMR (~160 ppm in Figure S16). Contribution from [Im]⁻-CO₂ (C) is very small, even in the absence of EG, in contrast to the report by Nie et al.¹⁹ (Figure S17).

Scheme 1. CO₂ binding to [Ch]⁺[Trz]⁻:EG.



CO₂ absorption at 1 bar and 25 °C by the Ch[±]PhOH, Ch[±]ImH, [Ch]⁺[Trz]⁻, and [Ch]⁺[CNpyr]⁻ based eutectic solvents are shown in **Figure 3a**, with Ch[±]ImH:EG (1:2) demonstrating the highest CO₂ gravimetric capacity. Considering that the major products, EG-CO₂ and Ch[±]-CO₂, were induced by proton displacement, the ease with which the displaced proton could re-displace the chemisorbed CO₂, amongst other factors, impacted their thermal swing regenerability via conventional heating. This is apparent with [Ch]⁺[Trz]⁻:EG (1:2) which was easily regenerated under N₂ at 50 °C, whereas Ch[±]ImH:EG (1:2) required higher temperature (i.e., 70 °C) under the same N₂ flow. **Figure 3b** further shows [Ch]⁺[Trz]⁻:EG (1:2) eutectic to be easily recyclable at 50 °C, with a working capacity greater than 80%. The slight capacity decrease in the consecutive cycles resulted from the incomplete first cycle regeneration. Another factor could be the potential volatilization of EG (< 3wt% loss in 1 hr at 50 °C; Figure S18). These choline-based eutectics had

similar capacities with existing eutectics (See Table S4), with $\text{Ch}^{\pm}\text{ImH}$ showing the highest capacity, among the systems studied, at 3.25 moles of CO_2 per kg solvent corresponding to 14 wt% gravimetric capacity. Under 5000 ppm CO_2 in N_2 feed, $[\text{Ch}]^+[\text{Trz}]^-:\text{EG}$ (1:2) demonstrated a capacity of 0.4 mol CO_2/kg as shown in **Figure 3c**, demonstrating the selectivity to CO_2 and the utility of these sorbents for CO_2 capture from dilute streams such as direct air capture. The chemisorbed CO_2 in this sorbent was easily desorbed by dielectric heating at 50 °C via MW. The MW regeneration of $[\text{EMIM}]^+[\text{CNpyr}]^- \text{IL}^{24}$ and aqueous amines²⁵ were demonstrated recently as an alternative to steam-based temperature-swing methods. However, this concept has not been demonstrated for eutectic solvents before. A higher desorption rate was achieved with MW-based regeneration compared to conventional heating as seen in **Figure 3d**. It suggests that higher working capacities (difference between absorbed and desorbed CO_2 in a cycle) can be achieved in a given amount of cycling time with MW. Further, reliance on fossil fuel burning for low-grade waste steam to increase the temperature can be eliminated with the use of electricity from renewable energy sources.

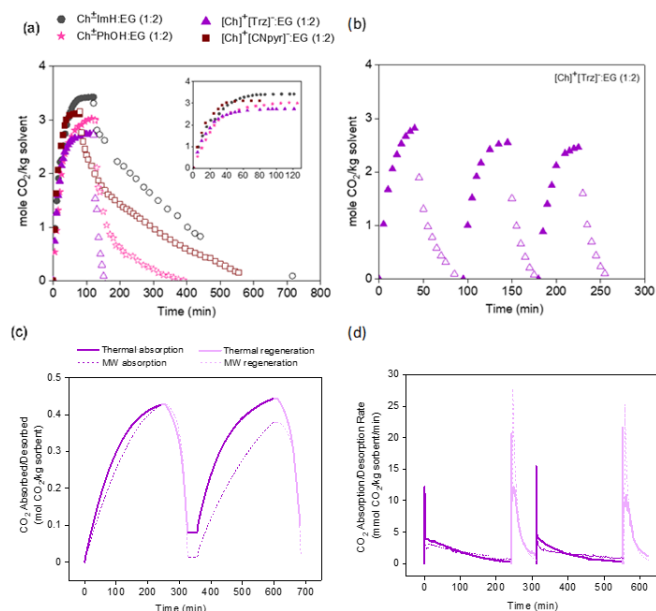


Figure 3. (a) CO_2 absorption by eutectic solvents at 1 bar of CO_2 and 25 °C and desorption under N_2 at 50 °C (70 °C for $\text{Ch}^{\pm}\text{ImH}:\text{EG}$ (1:2) only). Inset shows the absorption only. (b) Absorption-desorption cyclability of $[\text{Ch}]^+[\text{Trz}]^-:\text{EG}$ (1:2) with conventional thermal-swing. Filled and hollow symbols represent the absorption and desorption data, respectively (10% uncertainty).²⁶ (c) CO_2 absorption-desorption with $[\text{Ch}]^+[\text{Trz}]^-:\text{EG}$ (1:2) with conventional thermal- and MW-swing. Absorption at 5000 ppm CO_2 in N_2 ; desorption at 50 °C. (d) CO_2 absorption and desorption rates during MW-swing cycles.

In summary, an overall assessment of the functionalized choline-based eutectic solvents for CO_2 capture is presented in consideration of ease of synthesis, CO_2 capacity and selectivity, thermal stability, and regenerability via conventional thermal heating and microwaves. The importance of proton activity was evident from the examined CO_2 binding mechanism and strength as they relate to regenerability of the solvents for continued CO_2 absorption-desorption cycles. While the developed eutectic solvents were regenerable via both conventional thermal heating and dielectric heating, the working capacity achievable in a given amount of cycling time is

expected to be higher when MW is used due to the rapid desorption rate observed.

Acknowledgements

This study was supported by the U.S. Department of Energy, Office of Science, Basic Energy Sciences (award # DE-SC0022214). Partial support for DFT calculations by D.P. was from National Science Foundation, CBET (award # 1903259).

Conflicts of interest

There are no conflicts to declare.

Notes and references

- B. B. Hansen, S. Spittle, B. Chen, D. Poe, Y. Zhang, J. M. Klein, A. Horton, L. Adhikari, T. Zelovich, B. W. Doherty, B. Gurkan, E. J. Maginn, A. Ragauskas, M. Dadmun, T. A. Zawodzinski, G. A. Baker, M. E. Tuckerman, R. F. Savinell and J. R. Sangoro, *Chem. Rev.*, 2021, 121, 1232–1285.
- Y. Y. Lee, D. Penley, A. Klemm, W. Dean and B. Gurkan, *ACS Sustain. Chem. Eng.*, 2021, 9, 1090–1098.
- F. Y. Zhong, L. Zhou, J. Shen, Y. Liu, J. P. Fan and K. Huang, *ACS Sustain. Chem. Eng.*, 2019, 7, 14170–14179.
- Z. L. Li, F. Y. Zhong, J. Y. Huang, H. L. Peng and K. Huang, *J. Mol. Liq.*, 2020, 317, 113992.
- A. Klemm, S. P. Vicchio, S. Bhattacharjee, E. Cagli, Y. Park, M. Zeeshan, R. Dikki, H. Liu, M. K. Kidder, R. B. Getman and B. Gurkan, *ACS Sustain. Chem. Eng.*, 2022, 11, 3740–3749.
- Z. Wang, C. Wu, Z. Wang, S. Zhang and D. Yang, *Chem. Commun.*, 2022, 58, 7376–7379.
- S. B. Phadtare and G. S. Shankarling, *Environ. Chem. Lett.*, 2012, 10, 363–368.
- V. Agieienko and R. Buchner, *Phys. Chem. Chem. Phys.*, 2022, 17, 5265–5268.
- G. García, S. Aparicio, R. Ullah and M. Atilhan, *Energy and Fuels*, 2015, 29, 2616–2644.
- K. Zhang, Y. Hou, Y. Wang, K. Wang, S. Ren and W. Wu, *Energy and Fuels*, 2018, 32, 7727–7733.
- G. Cui, M. Lv and D. Yang, *Chem. Commun.*, 2019, 55, 1426–1429.
- S. K. Singh and A. W. Savoy, *J. Mol. Liq.*, 2020, 297, 112038.
- S. Li, Z. Zhou, Y. Zhang, M. Liu and W. Li, *Chem. Mater.*, 2005, 17, 5884–5886.
- C. Bunton and S. Diaz, *J. Am. Chem. Soc.*, 1976, 98, 5663–5671.
- S. Seo, M. A. Desilva and J. F. Brennecke, *J. Phys. Chem. B*, 2014, 118, 14870–14879.
- S. Zahn, B. Kirchner and D. Mollenhauer, *ChemPhysChem*, 2016, 17, 3354–3358.
- O. F. Mohammed, O.-H. Kwon, C. M. Othon and A. H. Zewail, *Angew. Chemie - Int. Ed.*, 2009, 121, 6369–6374.
- R. Li, Y. Zhao, Y. Chen, Z. Liu, B. Han, Z. Li and J. Wang, *Commun. Chem.*, 2018, 1, 1–8.
- M. N. Nie, Z. Wang, Q. H. Niu, J. X. Dai, Q. Q. Wang, J. S. Peng and P. Ji, *J. Org. Chem.*, 2023, 88, 5368–5376.
- F. G. Bordwell, *Acc. Chem. Res.*, 1988, 21, 456–463.
- C. Wang, X. Luo, H. Luo, D. E. Jiang, H. Li and S. Dai, *Angew. Chemie - Int. Ed.*, 2011, 50, 4918–4922.
- M. H. Nantz, L. Li, J. Zhu, K. L. Aho-sharon and D. Lim, *Biochim. Biophys. Acta - Lipids Lipid Metab.*, 1998, 1394, 219–223.
- L. Reuter and A. Lüchow, *Nat. Commun.*, 2021, 12, 4820.
- Y. Lee, E. Cagli, A. Klemm, Y. Park and R. Dikki, *ChemSusChem*, DOI:10.1002/cssc.202300118.
- S. Tsubaki, K. Furusawa, H. Yamada, T. Kato, T. Higashii, S. Fujii and Y. Wada, *ACS Sustain. Chem. Eng.*, 2020, 13593–13599.
- Q. Huang, Q. Luo, Y. Wang, E. Pentzer and B. Gurkan, *Ind. Eng. Chem. Res.*, 2019, 58, 10503–10509.